Pure Appl. Geophys. 177 (2020), 1295–1313

https://doi.org/10.1007/s00024-019-02410-1

Pure and Applied Geophysics

The Chios, Greece Earthquake of 23 July 1949: Seismological Reassessment and Tsunami Investigations

Nikolaos S. Melis,[1] Emile A. Okal,[2] Costas E. Synolakis,[3,4] Ioannis S. Kalogeras,[1] and Utku Kânoğlu[5]

Abstract—We present a modern seismological reassessment of the Chios earthquake of 23 July 1949, one of the largest in the Central Aegean Sea. We relocate the event to the basin separating Chios and Lesvos, and confirm a normal faulting mechanism generally comparable to that of the recent Lesvos earthquake located at the Northern end of that basin. The seismic moment obtained from mantle surface waves, $M_0 = 7 \times 10^{26}$ dyn cm, makes it second only to the 1956 Amorgos earthquake. We compile all available macroseismic data, and infer a preference for a rupture along the NNW-dipping plane. A field survey carried out in 2015 collected memories of the 1949 earthquake and of its small tsunami from surviving witnesses, both on Chios Island and nearby Oinousses, and on the Turkish mainland. While our results cannot help discriminate between the two possible fault planes of the 1949 earthquake, an important result is that both models provide an acceptable fit to the reported amplitudes, without the need to invoke ancillary sources such as underwater landslides, in contrast to the case of other historical tsunamis in the Aegean Sea, such as the 1956 Amorgos and 1948 Rhodos events.

Keywords: Aegean Sea, historical earthquakes, tsunami surveys.

1. Background and Previous Investigations

This paper provides a modern seismological investigation of the earthquake of 23 July 1949 on the Greek island of Chios, in the Aegean Sea. This event was given a "Pasadena" magnitude $M_{PAS} = 6\frac{3}{4}$, reported by various agencies, but not included in Gutenberg and Richter's (1954) generally authoritative catalog. This magnitude makes it the second largest instrumentally recorded historical earthquake in the Central Aegean Sea after the 1956 Amorgos event (Okal et al. 2009), a region broadly defined as limited to the South by the Cretan–Rhodos subduction arc and to the north by the western extension of the Northern Anatolian Fault system. The earthquake resulted in considerable damage, with several hundred houses destroyed in the northeastern villages of Chios Island and on the nearby Karaburun Peninsula in Turkey. As such, it ranks among the more destructive of the past hundred years in the Eastern Aegean Sea. Miraculously, only ten casualties were reported, as compiled from a detailed review of news reports performed during the present study.

The earthquake was accompanied by a small tsunami in northern Chios and the nearby island of Oinousses, with additional wave activity reported in Çeşme and on the Karaburun Peninsula (Fig. 1).

The 1949 earthquake was the subject of a study by Galanopoulos (1954), and more recently of a review by Altınok et al. (2005). Galanopoulos (1954) described the effects of the event on both the Greek and Turkish sides. In Greece, macroseismic observations consisted of filled questionnaires and telegrams, used to report back information to the National Observatory of Athens (NOA) from dedicated locally appointed personnel, especially on Chios Island Mr. Kreatsas, a physicist, who was at the time Director of the Chios Gymnasium. This information, and reports from Turkey, were then evaluated by Galanopoulos (1954) in terms of Mercalli-Sieberg Intensities (MSI) (Musson et al. 2010), and compiled into a map of the devastation on both sides of the

[1] Geodynamics Institute, National Observatory of Athens, P.O. Box 20048, 11810 Athens, Greece.
[2] Department of Earth and Planetary Sciences, Northwestern University, Evanston, IL 60208, USA. E-mail: emile@earth.northwestern.edu
[3] Department of Civil Engineering, University of Southern California, Los Angeles, CA 90089, USA.
[4] Environmental Engineering School, Technical University of Crete, 73100 Chania, Greece.
[5] Department of Aerospace Engineering, Middle East Technical University, 06800 Çankaya, Ankara, Turkey.

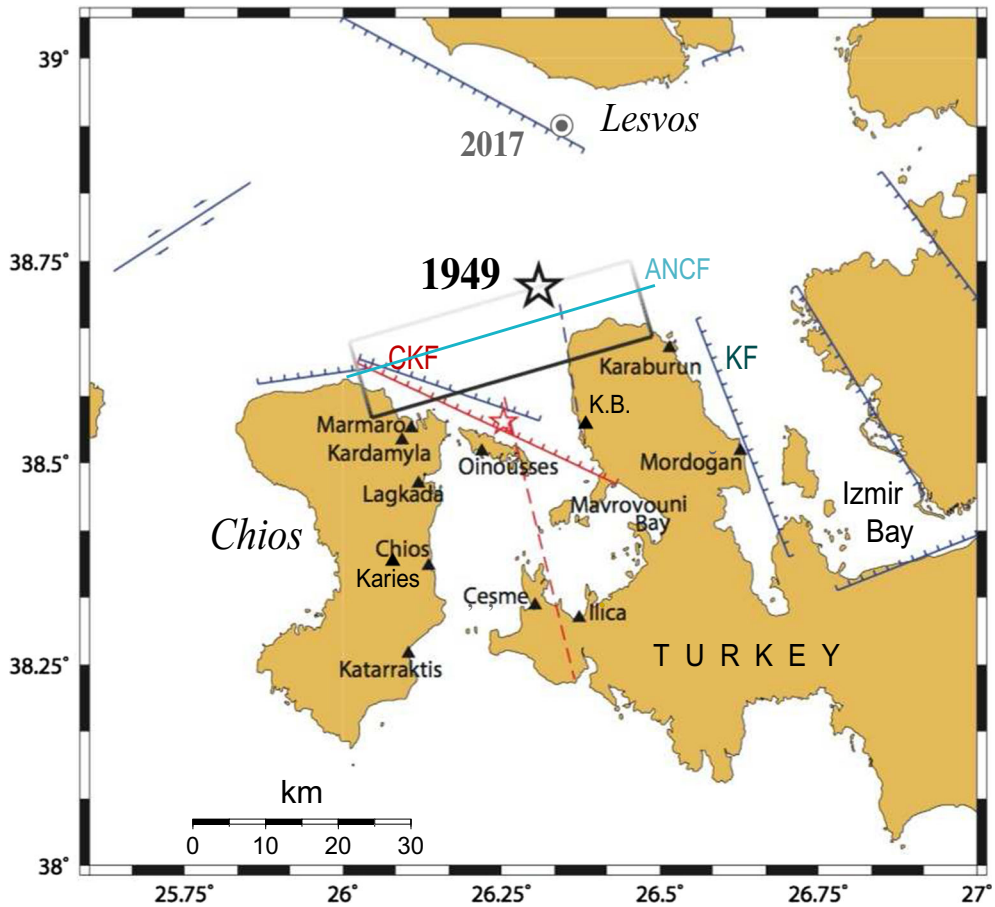

Figure 1

General location map of the 1949 Chios earthquake (large star). The rectangle shows the projection of our preferred rupture area. Also shown are the principal faults recognized or proposed in the area, notably the Chios–Karaburun fault (CKF), proposed by Galanopoulos (1954), the Karaburun Fault (KF) defining the Western boundary of the Izmir Bay, the unnamed offshore fault hosting the 2017 Lesvos earthquake, and in red dashes, another fault proposed by Galanopoulos (1954) as a possible site of the 1949 earthquake; the red star is his epicenter. The dark blue dashed line is the fault proposed by Altınok et al. (2005) along the northwestern coast of Karaburun Peninsula. Localities described in the text are shown as small triangles. *K.B.* Küçükbahçe Bucağı, site of an $VIII\frac{1}{2}$ MSI report on the Turkish side. The light blue line is the Ayasmaton-Northern Chios Fault (ANCF) identified in the GreDaSS database (Caputo et al. 2012). Adapted from Galanopoulos (1954), Altınok et al. (2005), Chatzipetros et al. (2013; Fig. 5a) and Kiratzi (2018; Fig. 2)

border, offered as Figure 2 of Galanopoulos (1954). Unfortunately, little information could be gleaned from local instrumental data, since at the time, there was only one seismic station (Athens, ATH) in operation in Greece; although it was well-equipped under the world-wide instrumental standards of the day, with one Mainka instrument (two horizontal components; $T_p = 5.8$ s), one horizontal two-component ($T_p = 9$ s) and one vertical ($T_p = 4$ s) Wiechert seismographs, their records were all saturated by the mainshock. Hence, Galanopoulos (1954) relied on the manual drafting of isoseismals, together with some knowledge of the local geomorphology and structural geology, to define the main fault responsible for the event and its relation to the epicenter. He favored a "Chios–Karaburun" WNW–ESE normal fault dipping towards NNE, with its hypothetical surface trace lying North of the coast of Chios and Oinousses, to the Western coast of the Karaburun Peninsula into the Mavrovuni (Gerence) Bay (Fig. 1).

Altınok et al. (2005) described the damage for both the 1881 and the 1949 events that took place South and North of the Chios-Çeşme and Chios–Karaburun areas, respectively, but mostly focused their reports on the Turkish side. Regarding the 1949 event, they used mainly a review of Galanopoulos (1954) and incorporated material from Pinar (1950) and Papazachos and Papazachou (1997), as well as from Turkish newspapers, which reported earthquake effects and damages nearly exclusively on the Turkish side, and in particular episodes of water jets gushing on the port of Çeşme. Altınok et al. (2005) adopted Galanopoulos' (1954) proposed Chios–Karaburun fault, which they complemented with an almost NW-SE striking hypothetical fault mapped in the sea and consistent with the geomorphology of the western coast of the Karaburun Peninsula. They do not add standard information on flooding (inundation, run-up) on the Turkish side.

In this context, the present paper presents a new, comprehensive, re-investigation of the 1949 Chios earthquake, including the building and modeling of a macroseismic database, a quantification of the seismic moment of the source and of its radiated energy, based on waveform analysis, and a tsunami simulation to model the results of a survey which involved the interview of elderly witnesses on both the Greek and Turkish sides. The latter sought to provide an independent validation of quantitative reports of inundation and flooding. As discussed in Sects. 4 and 5, its results were moderate, but can help to put general constraints on the seismic source of the 1949 event.

2. *Relocation and Background Seismicity*

We relocated the 1949 Chios earthquake based on arrival times listed in the International Seismological Summary (ISS), using Wysession et al.'s (1991) interactive, iterative method, which defines a confidence ellipse based on a Monte Carlo algorithm injecting Gaussian noise into the dataset; for an event in 1949, we give the noise a standard deviation $\sigma_G = 3$ s. Our relocation converges to 38.71° N, 26.32° E, approximately 25 km NNE of the Island of Oinousses (Fig. 2a). This solution is obtained at a constrained depth of 10 km. Attempts to keep the depth floating could not produce a stable positive hypocentral depth. This is confirmed by a weak, but systematic increase in r.m.s. residuals σ with hypocentral depth for constrained-depth relocations (Fig. 2b); at the same time, increasing constrained depth results in a northerly moveout of the epicenter (small dots on Fig. 2a), into an area close to Lesvos where only two small, poorly located events ($m_b \approx 3$) are claimed to have occurred deeper than 70 km in the past 50 years. We conclude that the 1949 earthquake was most probably shallow ($h \leq 30$ km), in agreement with trends in modern seismicity, as defined by NEIC solutions (1970–2015) reported within 30 km of our preferred epicenter and with at least one magnitude $M \geq 4.5$ (such events can be considered reliably located), for which the maximum depth is 31 km. Our results also agree with Galanopoulos' (1954) suggestion of a depth of 12–17 km for the 1949 earthquake, using the rapid decay of felt intensities with distance, as interpreted in the framework of Gutenberg and Richter's (1942) empirical relations.

Figure 2a also compares our solution with the epicenters originally given by the ISS, the U.S. Geological Survey and the Jesuit Seismological Association (JSA), those proposed by Erkman (1949), Labrouste and Pinar (1953), Galanopoulos (1954), Ambraseys (1998), or obtained by modern computerized relocations such as McKenzie's (1972), Ambraseys' (2001), or the ISC-GEM relocated epicenter (Storchak et al. 2013). Note that the earthquake is not part of Gutenberg and Richter's (1954) otherwise authoritative catalog (even though a "Pasadena" magnitude appears in the ISC bulletin), nor was it relocated as part of Engdahl and Villaseñor's (2002) Centennial catalog.

We note that modern relocations [such as by the ISC, McKenzie (1972), Ambraseys (2001) or this study] move the epicenter about 30 km North of the group of more ancient estimates, such those of the ISS, Erkman (1949), Labrouste and Pinar (1953), Galanopoulos (1954) or even Ambraseys (1988). In this context, it seems difficult to associate the earthquake with the proposed fault running WNW–ESE from North of Chios and Oinousses to the Southern tip of the Karaburun Peninsula (Galanopoulos 1954,

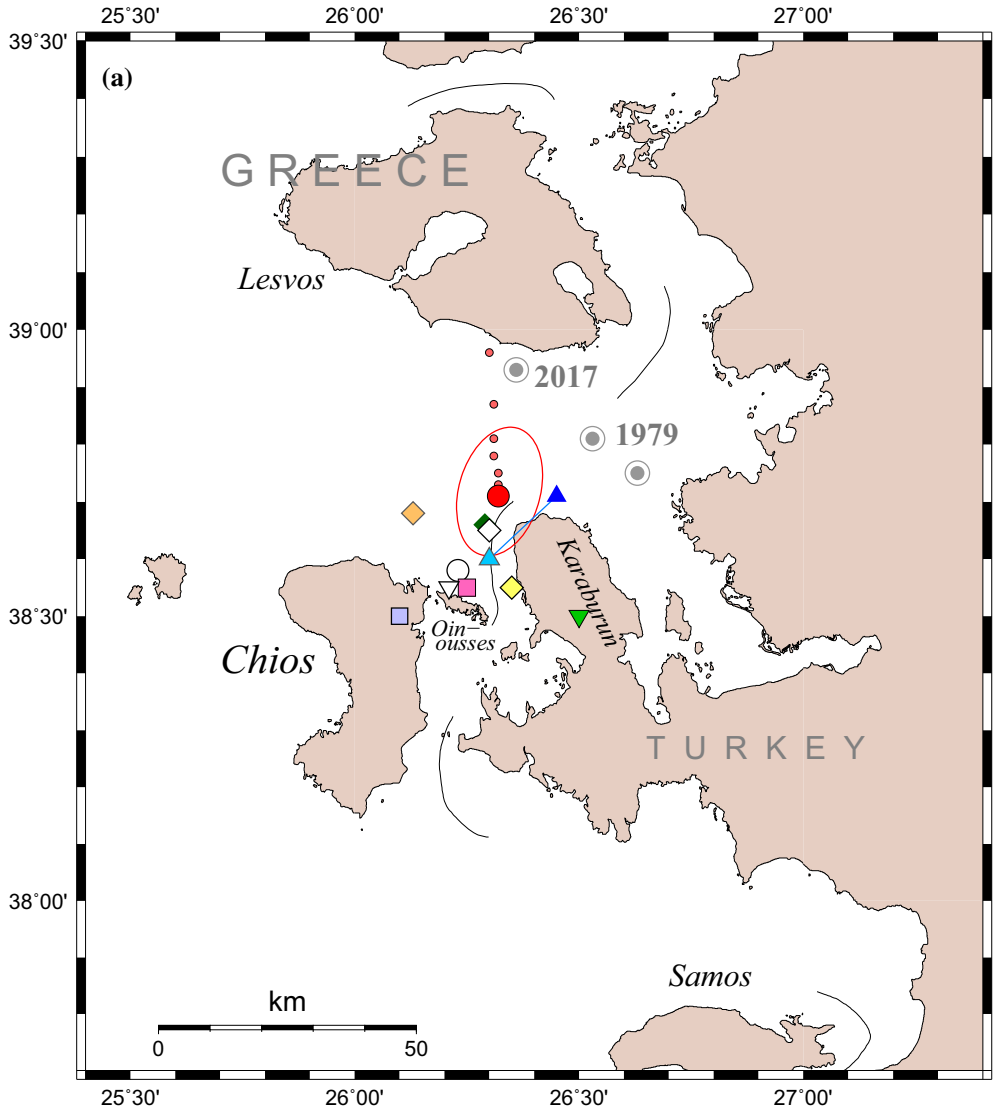
25°30'
26°00'
26°30'
27°00'
39°30'
39°00'
38°30'
38°00'
(a)
GREECE
Lesvos
2017
1979
Karaburun
Oin-
ousses
Chios
TURKEY
Samos
km
0
50

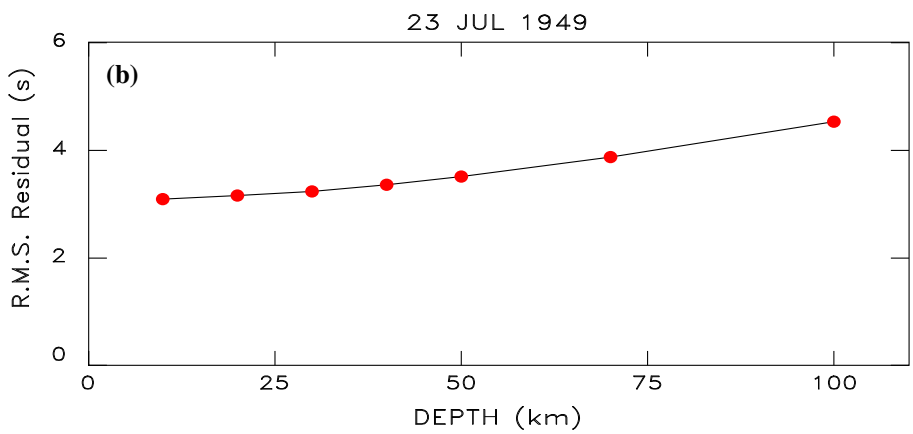
23 JUL 1949
(b)
R.M.S. Residual (s)
0
2
4
6
0
25
50
75
100
DEPTH (km)

◀Figure 2
a Relocation of the 1949 Chios earthquake. Our relocated epicenter is shown as the solid red dot, with Monte carlo ellipse; small dots indicate the moveout of the epicenter as depth is increased from 10 to 100 km. Other epicenters shown are: original ISS (light blue triangle); relocated ISC (dark blue triangle); USGS (green inverted triangle); JSA (light purple square); Galanopoulos (1954) (magenta square); Papazachos and Papazachou (1997) (light brown diamond); Labrouste and Pinar (1953) (yellow diamond); Erkman (1949) (open circle); Ambraseys (1988) (white open inverted triangle); Ambraseys (2001) (white open diamond); and McKenzie (1972) (dark green diamond). For reference, the 1979 and 2017 Lesvos earthquakes are shown as the grey bull's eye symbols. **b** R.M.S. residual as a function of constrained depth for relocations of the 1949 Chios earthquake

Figure 2). Rather, the emerging picture would associate the source with the faults named Ayasmaton and Northern Chios in the Greek Database of Seismogenic Sources (Caputo et al. 2012), and shown as the greenish blue line (ANCF) on Fig. 1.

Table 1 also lists the result of relocations of eight "associated" earthquakes originally listed as occurring in the Aegean Sea during the years 1949–1950. Of those, only Events A03 and A06 can be considered genuine aftershocks of the Chios earthquake. This meager number prevents an interpretation of aftershocks in terms of the extent of the fault zone of the mainshock. Event A05 is poorly located (with only 6 stations), but its Monte Carlo solutions run with unconstrained depths are peaked around 126 km, approximately 120 km South of the mainshock; similarly, Event A04, originally undetermined by the ISS, relocates to the Peloponese-Crete subduction system, with a most probable depth of 70 km. We have verified that modern seismicity exists at the proposed 3-D locations of Events A04 and A05. Two more events (F01 and A08) relocate on Lesvos, in the vicinity of the 2017 epicenter, and the remaining two earthquakes (A07 and A09) relocate in mainland Turkey. Figure 3 summarizes these results; no magnitude estimates are available, except $M_s = 5.1$, recomputed by the ISC for Event A09, and largely irrelevant to the present study.

3. *Focal Mechanism and Quantification of the Source*

3.1. *Focal Mechanism*

McKenzie (1972) listed a mostly normal focal mechanism ($\phi = 141°$, $\delta = 65°$, $\lambda = 321°$), based on Wickens and Hodgson's (1967) catalog of focal solutions (Fig. 4). We verified this mechanism through an independent examination of historical seismograms, which allowed us to obtain 14 first motion polarities. These are plotted as large symbols

Table 1

Relocations carried out in the present study

Code	Date	Relocation								Notes
(*)	D M (J) Y	Origin time	Epicenter		Depth		Nr. of stations		σ	
			(°N)	(°E)	(km)	(**)	Read	Kept	(s)	
F01	21 MAY (141) 1949	17:41:18.5	39.05	26.07	67	F	16	13	4.96	Lesvos
M02	**23 JUL (204) 1949**	**15:03:32.5**	**38.71**	**26.32**	**10**	**C**	**132**	**129**	**3.10**	**Mainshock**
A03	30 JUL (211) 1949	17:47:12.6	38.73	26.35	60	F	35	32	4.13	Genuine aftershock
A04	01 AUG (213) 1949	15:27:36.8	35.32	22.31	67	F	21	11	3.98	Southern Greece
A04	01 AUG (213) 1949	15:27:36.8	35.32	22.31	67	F	21	11	3.98	Southern Greece
A05	01 AUG (213) 1949	22:42:26.9	37.77	26.30	126	C	7	6	2.89	Aegean Sea; Deep
A06	23 NOV (327) 1949	16:51:01.4	38.60	26.23	33	F	54	51	3.32	Genuine aftershock
A07	03 MAY (123) 1950	07:13:43.1	38.66	27.16	10	C	28	25	4.02	Gediz Valley, Turkey
A08	08 JUL (189) 1950	07:07:24.2	39.10	26.31	10	C	13	11	3.72	Lesvos
A09	28 NOV (332) 1950	17:53:20.5	39.69	28.17	33	F	32	30	3.77	Balıkesir, Turkey
			For reference							
L10	12 JUN (163) 2017	12:28:04.9	38.81	26.2	12					2017 Lesvos Event

(*) *F* Foreshock, ***M*** **Mainshock**, *A* Aftershock, *L* Lesvos event (2017)

(**) *C* Constrained depth, *F* Floated depth

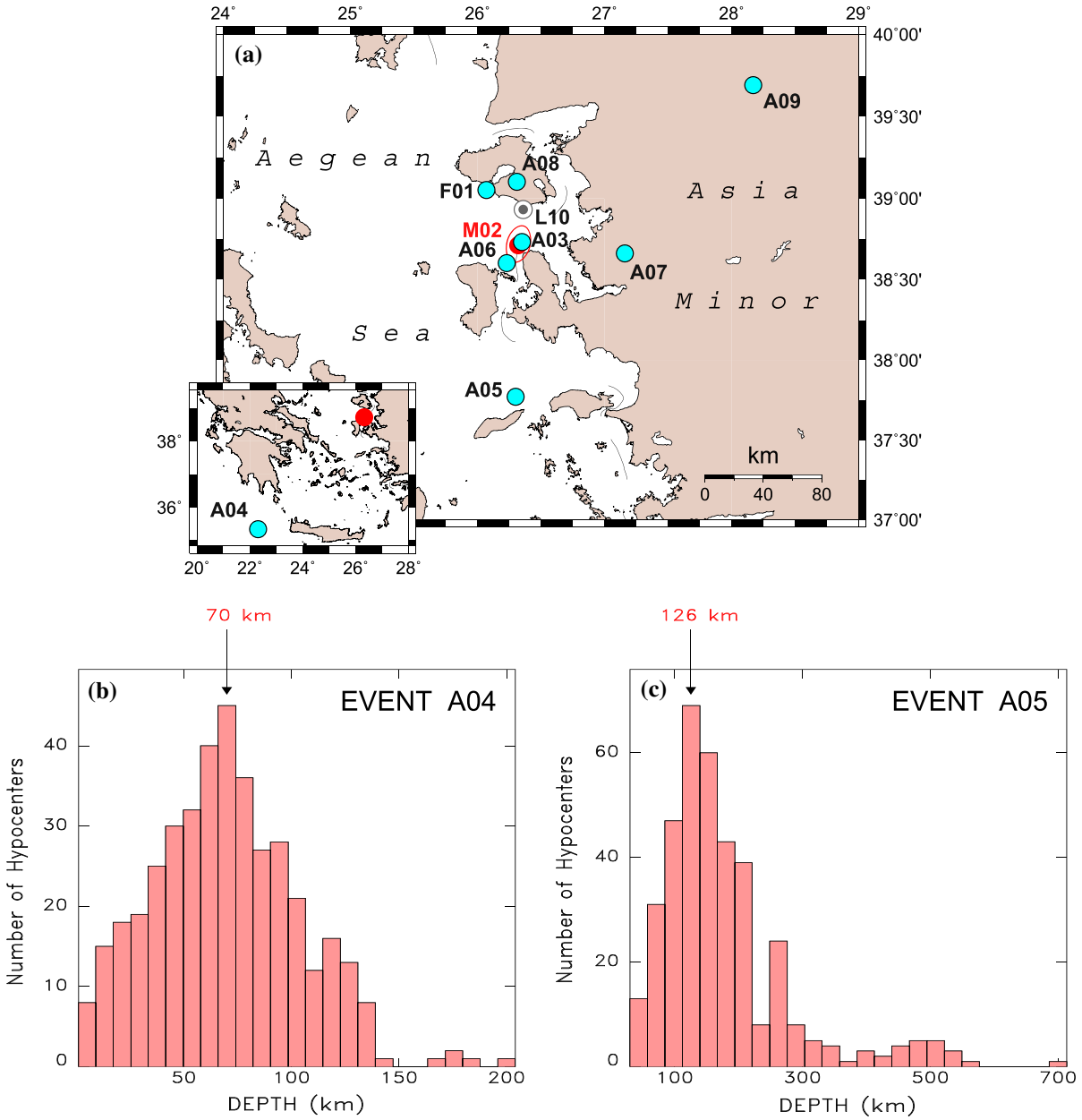

Figure 3

a Relocations of associated earthquakes, as listed in Table 1. The red dot shows the mainshock (M02) with its Monte Carlo ellipse. **b** Histogram of hypocentral depths inverted from the Monte Carlo algorithm for Event A04, suggesting a 70–km deep source inside the subducting slab of Southwestern Greece; **c** same as **b** for Event A05, suggesting a 126-km deep source

on Fig. 4a, together with 10 polarities reported in the ISS (smaller symbols); all details are provided in Table 2. On this basis, we propose the mechanism $\phi = 254°$, $\delta = 57°$, $\lambda = 218°$ (conjugate mechanism $\phi = 141°$, $\delta = 59°$, $\lambda = 320°$), rotated only 6° from McKenzie's (1972) in the formalism of Kagan (1991). This mechanism also shares its normal faulting character with the composite solution ($\phi = 249°$, $\delta = 47°$, $\lambda = 259°$), proposed by Karakostas et al. (2010; Figure 6 and Table 1) for a

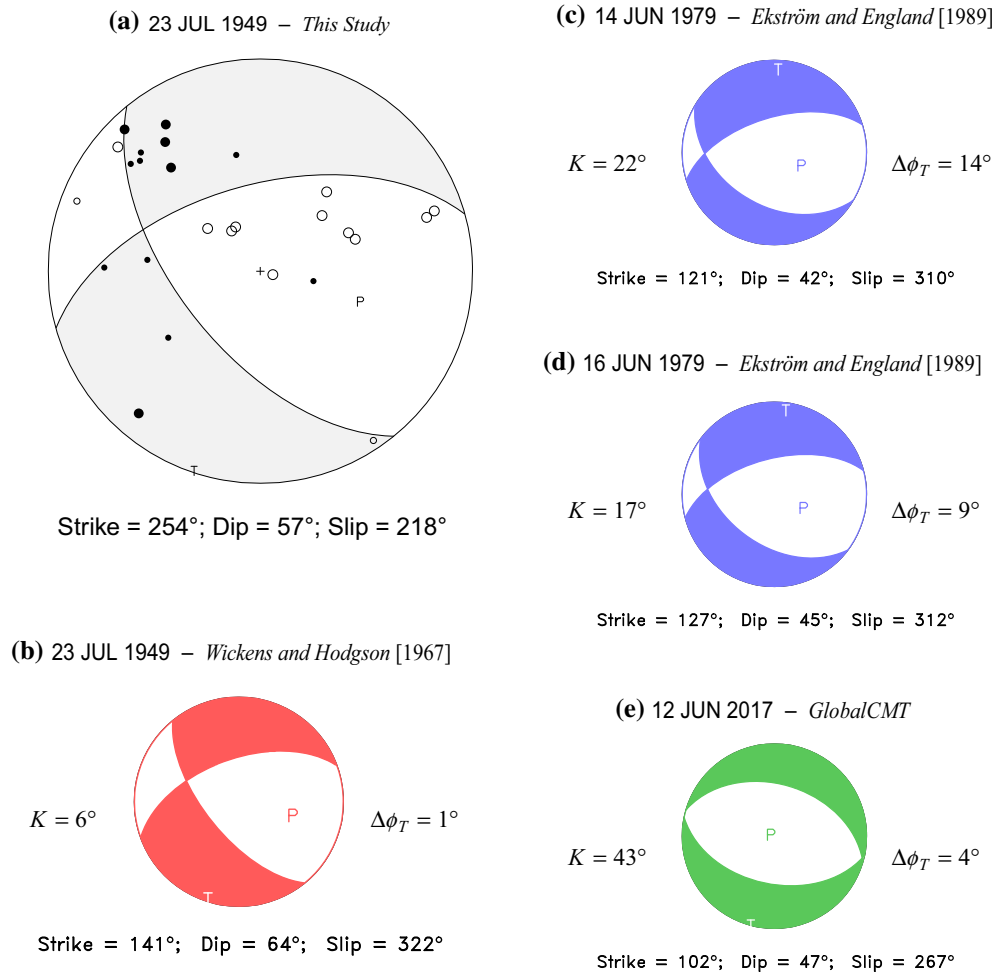

Figure 4
Top left: focal mechanism obtained in this study for the 1949 Chios earthquake. Full symbols are anaseismic arrivals, open ones kataseismic; large symbols read as part of this study, small ones transcribed from the ISS, as listed in Table 2. Bottom left: mechanism proposed by Wickens and Hodgson (1967). Right: published mechanisms for neighboring earthquakes in the vicinity of Lesvos. For the four referenced mechanisms, we give, with respect to our solution, the solid rotation angle K in the formalism of Kagan (1991), and the difference $\Delta\phi_T$ in the azimuths of tensional axes (always sub-horizontal)

cluster of recent low-level seismicity centered about 15 km South of our relocated epicenter.

On Fig. 4, we further compare the 1949 mechanism with those of the nearby 2017 Lesvos earthquake, and of two 1979 earthquakes, studied by Ekström and England (1989), $\sim$30 km to the Southeast of Lesvos. All feature normal faulting, and a mechanism very close to that of the 1949 earthquake, as measured by the angle K of solid rotation separating them in the formalism of Kagan (1991). Even more remarkable is the agreement between tensional axes **T**, all being sub-horizontal and differing at most 14° in azimuth.

This general pattern of consistent tensional axes in the region was pointed out by Taymaz et al. (1991) from a compilation of generally smaller events. It expresses the deformation of the Aegean Basin upon the transformation of strike-slip motion between Asia Minor and Eurasia, notably along the North Anatolian Fault, to the collisional regime between the African plate and the Aegean basin at the Hellenic Arc to the South.

Table 2

First motion data used in the focal mechanism study

Station		Polarity (*)	Distance (°)	Azimuth (°)
Name	Code			
Read on original seismograms				
Athens, Greece	ATU	k	2.17**	250.9
Istanbul, Turkey	IST	a	3.11**	40.5
Zagreb, Croatia	ZAG	a	10.43	316.2
Trieste, Italy	TRI	k	11.63	311.0
Prague, Czech Republic	PRA	a	14.16	327.2
Tbilisi, Georgia	TIF	k	14.42	72.1
Göttingen, Germany	GTT	a	17.20	323.6
De Bilt, The Netherlands	DBN	a	19.88	319.2
Yekaterinberg, Russia	SVE	k	28.85	39.9
Toshkent, Uzbekistan	TAS	k	32.73	71.5
Almaty, Kazakhstan	AAA	k	37.95	66.4
Irkutsk, Russia	IRK	k	53.65	48.1
Harvard, Massachusetts	HRV	k	70.01	308.9
Tucson, Arizona	TUC	k	98.71	324.4
Pasadena, California	PAS	k	100.22	330.7
Wellington, New Zealand	WEL	k	155.79***	106.2
Additional data reported by the ISS				
Belgrade, Serbia	BEO	k	7.51**	326.3
Rome Monte Porzio, Italy	RMP	k	10.84	290.9
Zürich, Switzerland	ZUR	a	15.55	309.5
Stuttgart, Germany	STU	a	15.90	314.8
Strasbourg, France	STR	a	16.61	312.5
Algiers, Algeria	ALG	a	18.47	271.3
Uppsala, Sweden	UPP	a	21.86	348.2
Cartuja, Spain	CRT	a	23.57	275.7
Tamanghaset, Algeria	TAM	a	23.82	234.2
Jakarta, Indonesia	BAT	a	86.46	100.8

Station names reflect present spelling and political boundaries

(*) a: anaseismic (first motion up); k: kataseismic (first motion down)

(**) Station maps onto upper focal hemisphere

(***) Core phase (PKP)

3.2. Seismic Moment

We quantified the seismic moment of the 1949 Chios earthquake from records of mantle surface waves at the teleseismic stations listed in Table 3, with representative examples of waveforms shown on Fig. 5. The records were digitized and processed through the M_m algorithm (Okal and Talandier 1989), with results shown on Fig. 6 in the form of the variation with frequency of the mantle magnitude, corrected for focal mechanism and depth, related to seismic moment through:

$$M_c = \log_{10} M_0 - 20 \qquad (1)$$

where M_0 is in dyn cm. Figure 6 shows a slight growth of moment with decreasing frequency (with a slope of -0.07 logarithmic units per mHz) and suggests a value of 7×10^{26} dyn cm at the longest sampled periods (170–200 s).

3.3. Macroseismic Modeling

We resolved the indeterminacy between the two fault planes on Fig. 4a by modeling the field of macroseismic data. Galanopoulos (1954, Figure 2) provided an original compilation of isoseismals and described widespread destruction corresponding to Mercalli-Sieberg Intensity VIII in the Northern part

Table 3

Surface wave records used in the moment determination

Station	Code	Distance (°)	Azimuth (°)	Instrument type	Mantle waves used
De Bilt, The Netherlands	DBN	19.9	319.2	Golitsyn	G_1, R_1
San Juan, Puerto Rico	SJG	80.7	285.9	Wenner	G_1, R_1
Tucson, Arizona	TUC	98.7	324.4	Benioff 1-77	R_1
Pasadena, California	PAS	100.2	330.8	Benioff 1-90	G_1

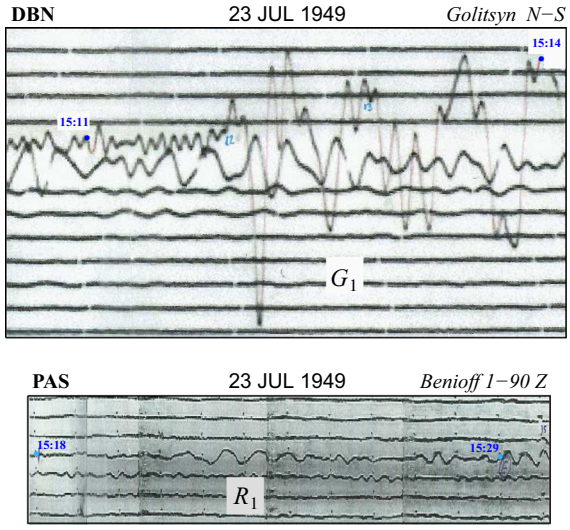

Figure 5
Representative waveforms used in the determination of the seismic moment of the 1949 Chios earthquake. Top: Love wave recorded on the Golitsyn N–S instrument at De Bilt, The Netherlands. Bottom: Rayleigh wave recorded on the Benioff 1–90 vertical instrument at Pasadena

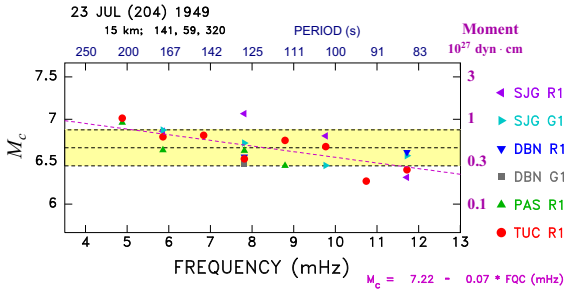

Figure 6
Mantle magnitudes computed for the 1949 Chios earthquake. The horizontal scale is linear in frequency. The horizontal dashed line is the average magnitude corrected for focal mechanism, M_c (Okal and Talandier 1989) and the yellow band its 1–σ confidence interval. Equivalent moments (logarithmic scale) shown at right. The purple dashed line (and equation at *bottom right*) is a linear regression of M_c with frequency

of Chios (reaching IX in Kardamyla), with several villages devastated. He also documented a comparable level of destruction in the Northern part of the interior of the Karaburun Peninsula in Turkey.

In this study, we re-examined all telegrams, completed questionnaires and newspaper clippings and other unpublished material available as part of the NOA Bulletin Library. At each reporting location, a new Modified Mercalli Intensity (MMI) was assigned, and the material converted into a homogeneous dataset of macroseismic intensities, listed in Table 4 (see "Appendix"). The resulting dataset was smoothed using a kriging technique (Schenková et al. 2007; Linkimer 2008), and is presented in Fig. 7a, b. We note that, even though the earthquake was reported felt on Lesvos, 40 km to the North, there were no reports of destruction, indicating an intensity of only VI on the Mercalli-Sieberg or Modified Mercalli scales.

Based on the long-period seismic moment of 7×10^{26} dyn cm, we use Geller's (1976) scaling laws to derive a rupture length $L = 40$ km, a width $W = 20$ km, and a seismic slip $\Delta u = 1.2$ m. For each of the two possible fault planes, we position the top of the fault at a depth of 5 km below the Earth surface, and use the Scenario Shake Map Calculator (Field et al. 2005) to compute a field of maximum ground accelerations, which are then converted to Modified Mercalli Intensities.

Results are shown on Fig. 7c, d. It is clear that the use of the NNW-dipping plane ("Model 1"; $\phi = 254°$, $\delta = 57°$, $\lambda = 218°$; Fig. 7c) adequately reproduces the concentration of maximum intensities in the Northern part of Chios, with similar intensities in Northern Karaburun. By contrast, the SW-dipping plane ("Model 2"; $\phi = 141°$, $\delta = 59°$, $\lambda = 320°$; Fig. 7d) results in weaker intensities, not exceeding VII in Northern Chios, with the field of Intensity VIII

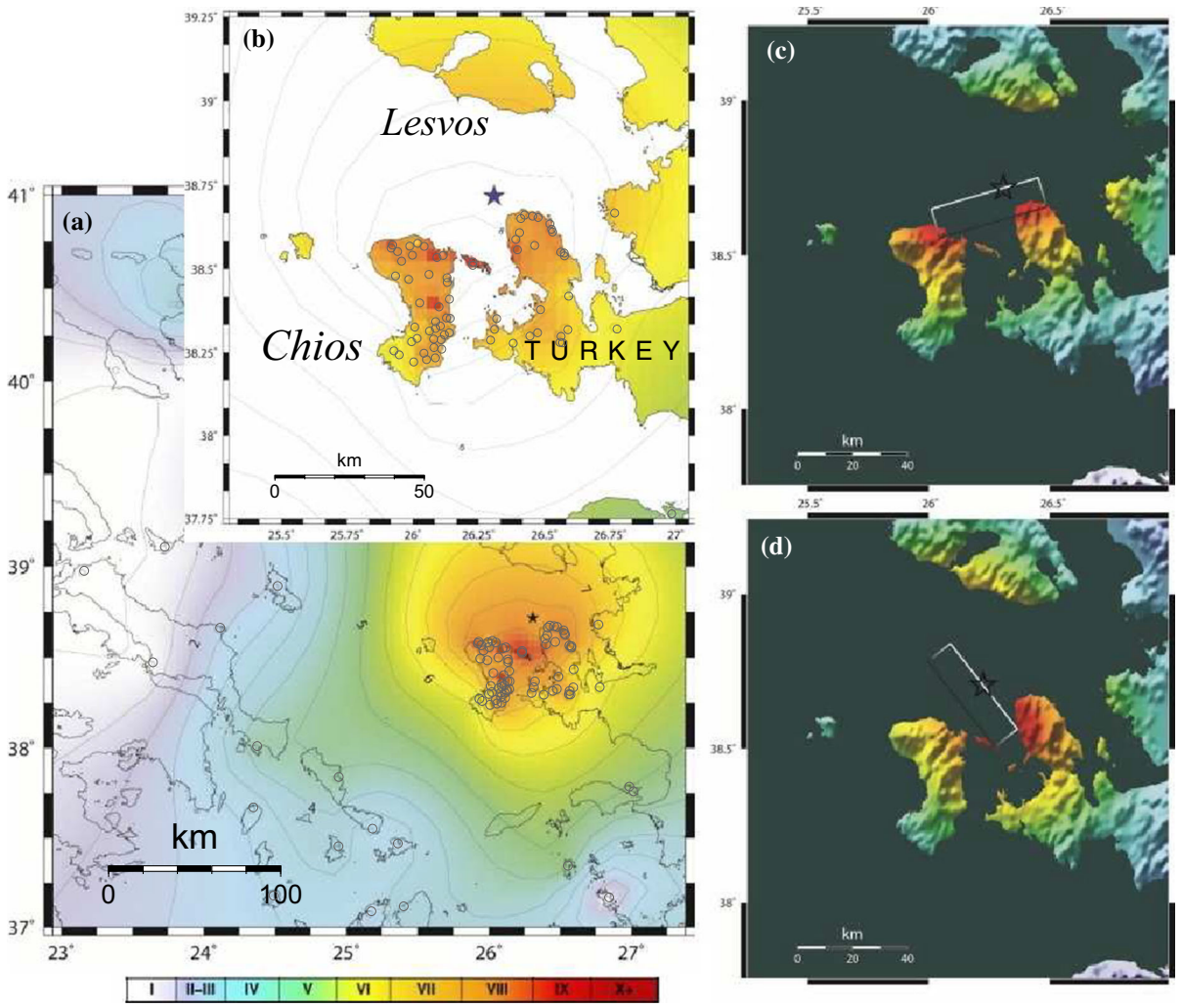

Figure 7

Macroseismic dataset and modeling. **a** Map of the dataset obtained in this study. Individual points shown as circles color-coded according to their MSI value. The background shading is the result of the kriging procedure for the entire Aegean Sea. **b** Close-up of **a** with shading restricted to land masses. Note highest MSI values (VIII$\frac{1}{2}$ to IX) restricted to Northern Chios, one inland location (Karies), Oinousses, and one location on the Western Coast of Karaburun (Küçükbahçe Bucağı), and low values (VI$\frac{1}{2}$ to VII) at Lesvos. **c** Field of MSI values predicted for Model 1 by the Scenario Shake Map Calculator. The rectangle shows the projection of the rupture area and the star denotes the epicenter. **d** Same as **c** for Model 2. Note better agreement of Model 1 with dataset in **b**

restricted to Karaburun, in contradiction with the field data (Fig. 7a). Note that both predict weak intensities, not exceeding VI on the Southern coast of Lesvos. On this basis, we prefer to interpret the NNW-dipping plane as the fault plane.

We note that this plane defines the Southern boundary of the Lesvos Basin, which reaches a depth of 800 m between the islands of Lesvos and Chios. The basin is limited to the North by the unnamed SSW-dipping normal fault along which the 2017 Lesvos earthquake took place (Kiratzi 2018). The combination of the two facing normal faults takes up the local tensional regime in the general "telephone book" model of Taymaz et al. (1991).

Finally, given the poor depth control of our relocations, we have examined the effect on our macroseismic modeling of deepening the seismic source by 20 km, thus keeping it within the range of

acceptable solutions suggested by Fig. 2b, but at the same time keeping all other source parameters (seismic moment, focal mechanism, source dimensions). Not surprisingly, we found that the modeled intensities are significantly lower (by about two units) for the deep source, with a maximum of MMI VII, which does not reproduce the intensities compiled in Table 4 and described by Galanopoulos (1954). These results thus confirm the shallow character of the source.

3.4. Source Slowness and Parameter Θ

We further investigated the possible existence of slowness in the source of the 1949 Chios earthquake through the parameter Θ introduced by Newman and Okal (1998) in the framework of Boatwright and Choy's (1986) methodology:

$$\Theta = \log_{10} \frac{E^E}{M_0} \qquad (2)$$

where E^E is the estimated seismic energy radiated into teleseismic body waves, which is obtained by integrating the energy flux at a receiver station. Earthquakes following scaling laws are expected to feature $\Theta = -4.90$; lower values, typically $\Theta < -5.80$, are characteristic of source slowness, as featured by "tsunami earthquakes" (Kanamori 1972; Newman and Okal 1998); by contrast, higher values, typically $\Theta > -4.50$ are typical of "snappy" earthquakes, in particular intraplate events featuring higher stress drops. The method can be successfully applied to historical earthquakes (e.g., Okal and Kirby 2002; Okal and Borrero 2011), as long as adequate short-period teleseismic records are available. In the present case, we obtained short-period records at Harvard (HRV) and Tucson (TUC). At TUC, the epicentral distance of 98.7° warrants a special correction; following Okal and Saloor (2017), we use a nearby reference event, in this case the Lesvos earthquake of 12 June 2017, whose epicenter is only 25 km from the 1949 one and with a normal faulting mechanism rotated only $K = 39°$ (out of a possible 120°) in the formalism of Kagan (1991). We compute a value of $\Theta = -4.78$ for the Lesvos event, globally averaged using stations at standard distances, and then use regional values from a dense network at greater distances in Western North America, to define an empirical distance correction beyond 85° ($Corr. = 0.0923 \times \Delta - 8.04$), which we then apply to the 1949 record at TUC ($Corr. = 1.07$). We use the instrument response documented for 1947 at TUC by Okal and Saloor (2017) to obtain a final value $\Theta = -4.44$, shown as the centered blue square on Fig. 8. On the other hand, the station at HRV is at an appropriate distance (70.0°), but the gain of the instrument suffers from uncertainty (Ishii, pers. comm., 2018); the value of 25,000 reported by Charlier and van Gils (1953) would yield $\Theta = -4.87$, a significantly lower value than at TUC. At any rate, none of the two available records confirms the trend towards slowness suggested by the mantle wave study and which could affect the tsunami generation. The tentative value at HRV (−4.87) fits world-wide averages (−4.80; −4.98) and the theoretical value (−4.90) predicted by scaling laws Boatwright and Choy 1986; Newman and Okal 1998); the one at TUC (−4.44), probably more reliable on account of better constraints on instrumental response, would characterize the 1949

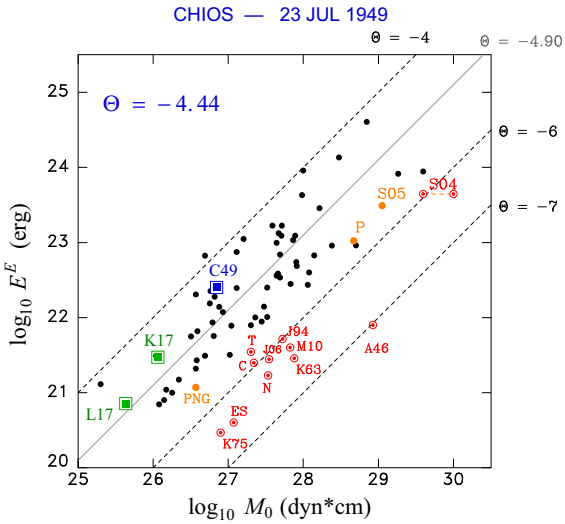

Figure 8
Energy vs. Moment and parameter Θ for the 1949 Chios earthquake (C49; shown in blue). The diagonal lines correspond to constant Θ. The points in the background constitute a selection of significant earthquakes of the past 25 years; "tsunami earthquakes" featuring Θ deficient by as much as 1.5 logarithmic unit, are shown in red. See Okal and Saloor (2017; Figure 13) for a complete list of labels. The 2017 Aegean events at Lesvos (L17) and Kos (K17) are shown in green

earthquake as "snappy", and is in general agreement with global values obtained in this study for the nearby 2017 Lesvos and Kos earthquakes (− 4.78 and − 4.59, respectively; see Fig. 8), which also featured comparable focal mechanisms. The apparent discrepancy between our surface wave results, which would advocate a trend towards slowness, and the energy estimated from *P* waves, which supports a snappy character for the source, can be reconciled by the presence of a high-frequency wavetrain (peaked at 2 Hz) in the TUC record, arriving about 40 s into the time series of the *P* wave, the resulting interpretation being a complex source with a later, more impulsive component.

4. Tsunami Field Survey

A field survey was conducted on 14–16 July 2015, which aimed at recording memories of elderly witnesses of the 1949 earthquake and tsunami. Its methodology followed our experience in previous surveys of historical tsunamis (e.g., Okal et al. 2002, 2009, 2015). We were able to interview a total of about 30 witnesses in the towns of Chios, Lagkada, Marmaro, Katarraktes (Chios); Oinousses; and Çeşme, Ilıca and Mordoğan (Karaburun Peninsula, Turkey); these locations are shown on Fig. 1. In the days following the event, local newspapers provided descriptions of wave activity, mentioned by Galanopoulos (1954); this information was later reproduced in Ambraseys (1988), Papazachos and Papazachou (1997), Altınok et al. (2005) and Solov'ev et al. (2013). Through the systematic interview of elderly witnesses, we sought to confirm, or as the case would be infirm, these reports.

On the island of Chios and in very general terms, our witnesses had vivid memories of the destruction caused by the earthquake, and accurately reported its main effects as having occurred in the northeastern villages, but none of them described flooding in the port of Chios, contrary to the description of a 2-m run-up by the national newspaper *Akropolis* (27 July 1949), later transcribed by Papazachos and Papazachou (1997), and referred to by Altınok et al. (2005), but revealed as incorrect by Papadopoulos (2015).

Similarly, none of our witnesses had any recollection of a significant subsidence of the port of Chios city, contrary to the report in *Vatan* (35 cm) mentioned by Altınok et al. (2005). We note that Model 1, preferred by our macroseismic study, would predict a slight *uplift* of only a few cm at that location, while Chios City would sit on a neutral line experiencing less than 1 cm vertical displacement under Model 2. It is thus probable that the report in *Vatan* relates to a destruction of port infrastructure by the shaking, rather than to a static subsidence.

The only reference to wave activity on the island of Chios was the confirmation of the oscillation of water, with an amplitude of 70 cm, at Marmaro, originally mentioned by Galanopoulos (1954), and reproduced in later publications. It was interpreted as seiching of the local bay, $\sim$1.8 km by 0.7 km in dimensions by Altınok et al. (2005).

On the Karaburun peninsula, we were able to interview a number of elderly residents in the villages of Ilıca and Mordoğan, as well as in Çeşme. One of our witnesses (75 years old in 2015, or 9 years at the time of the event), described structural damage to houses in Alaçatı where she lived at the time, and reddish water sprouting to a height of about 6 m on Ilıca beach, a phenomenon reported in the local press at the time of the event, and mentioned by Altınok et al. (2005). However, our witnesses mentioned no significant flooding or standard wave activity on the beach, a conclusion upheld by a careful examination of the local newspaper *Akşam*, which documents sprouting (which we have confirmed with an original photograph), but not flooding. In the town of Mordoğan, two witnesses (aged 8 and 15 at the time of the event) similarly mentioned co-seismic destruction but no wave activity, even though one of them also described rockslides falling into the sea, which apparently did not create observable waves.

Finally, we visited the island of Oinousses on 16 July 2015, where no reports of tsunami activity were mentioned in the local press at the time of the event. We were able to interview eight elderly witnesses, aged 77–82 years (11–16 in 1949). Based on one testimony, we measured a run-up of 0.32 m at the natural level of the quay along the port (a modern quay has since been built 50 cm taller); another witness who was riding a bicycle during the

earthquake, along the coastal road to the Merchant Marine School, about 1 km to the West of the port, described a withdrawal of the sea, with an amplitude of $\sim$35 cm. Yet another witness, who was at the time of the earthquake docking his boat at the Eastern end of the island (estimated location 38.514° N, 26.261° E) described having seen water springing to a reported height of 2 m between the two small islets of Gaidouroniso and Pontikonisi at an estimated position of 38.504° N, 26.270° E); however, we regard this height as tentative, given the distance of 1.4 km at which it was observed. We were unfortunately unable to visit those locations.

The dataset of confirmed tsunami amplitudes thus consists of: (1) a run-up of 32 cm at the port of Oinousses (38.514° N, 26.261° E); (2) a seiche of 70 cm amplitude in the Bay of Marmaro (38.546° N; 26.113° E); (3) no documented reports of wave activity (which we interpret as amplitudes probably less than 30 cm) at Chios City and on the Turkish coast (outside of observations of water locally springing from the ground at heights possibly reaching several meters). While this dataset remains meager, we will see that it can be reasonably well simulated by a model derived from our seismological observations.

5. *Tsunami Simulations*

Tsunami simulations were performed using the ComMIT package which was developed by Titov et al. (2011) as a graphical interface to the MOST finite differences algorithm (Titov and Synolakis 1998; Titov et al. 2016). MOST solves the shallow water approximation of the non-linear equations of hydrodynamics, using the method of alternated steps (Godunov 1959). It has been extensively validated through comparisons with laboratory and field data, per standard international protocols; full details can be found in Synolakis (2003) and Synolakis et al. (2008). In the present context, and since ComMIT allows the simulation of the inundation of initially dry land, time series at our virtual gauges are representative of flow depth at the coast line, as previously used in Greece, e.g., by Melis et al. (2016).

We use a bathymetric grid obtained from the European Marine Observation and Data Network (EMODnet), sampled at 30 m. Seismic sources consist of Models 1 and 2, as defined in the macroseismic study in Sect. 3 above, with fault geometries $\phi = 254°$, $\delta = 57°$, $\lambda = 218°$ for the NNW-dipping plane ("Model 1"), and $\phi = 141°$, $\delta = 59°$, $\lambda = 320°$ for the SW-dipping one ("Model 2"). In both instances we use a slip $\Delta u = 1.2$ m on a 40 km $\times$ 20 km fault. Initial displacements are calculated using the static deformation algorithm of Mansinha and Smylie (1971).

We then position three virtual gauges at the harbors of Chios Town, Oinousses and Marmaro. Figure 9 plots in red the time series simulated at the three gauges for Model 1, which uses the WSW–ENE striking plane and is preferred on the basis of the macroseismic data, and in blue for Model 2, which uses the NW–SE striking plane. We note that the

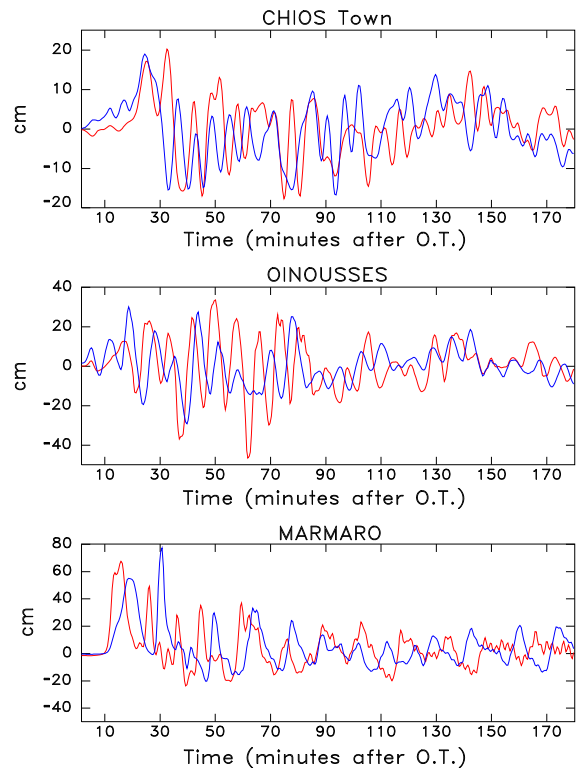

Figure 9
Simulated time series at the virtual gauges in the harbors of Chios Town (top), Oinousses (center), and Marmaro (bottom) for Models 1 (in red) and 2 (in blue). Note that maximum amplitudes for both models are comparable at each location

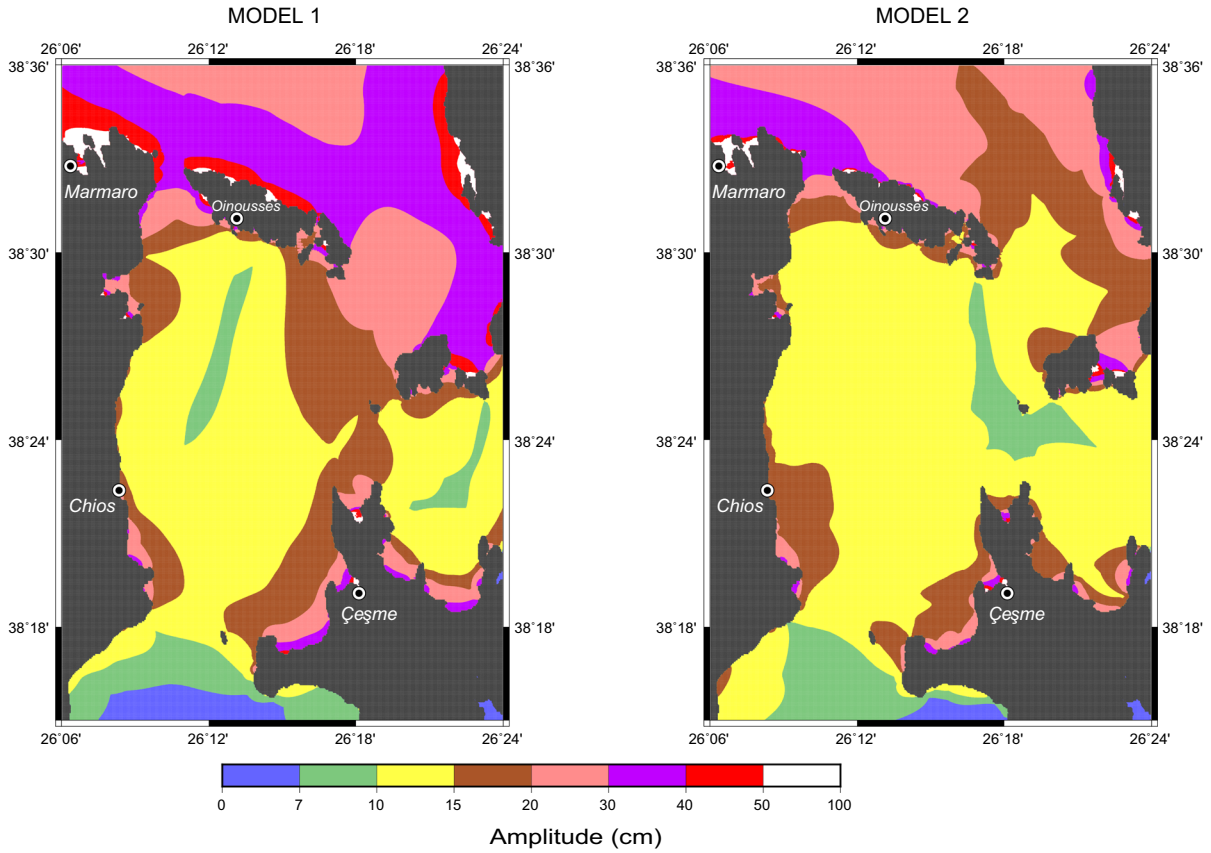

Figure 10
Results of hydrodynamic simulation for Models 1 (left) and 2 (right). In both cases, the field of maximum amplitudes of the tsunami is contoured using the same palet. Note that both models produce comparable amplitude fields, expect for larger η_{max} for Model 1 North of Oinousses and West of the Karaburun Peninsula. The bull's eye symbols identify the locations contributing to the database, occasionally slightly displaced so as not to mask simulation details

resulting amplitudes remain comparable at the three locations, and thus cannot be used to discriminate between the models: both reproduce well the amplitudes resulting from our survey (34 cm at Oinousses and $\sim$70 cm at Marmaro); at Chios Town, the simulated amplitudes (20 and 19 cm, respectively) are generally compatible with the lack of reports by our witnesses, notably given the significant level of destruction by the earthquake.

Figure 10 further shows a map of the maximum simulated wave amplitude η_{max} in our study area. Again, we note that results from the two models are very similar, with differences concentrated on the Northern coast of Oinousses, which is rugged and unpopulated, even to this day, as well as along the Northwestern coast of Karaburun, notably at the 2-km long bay South of Küçükbahçe Bucağı, a location also unpopulated in 1949. In this context, we must conclude that the evidence retrieved during our field survey is insufficient to discriminate between the two fault models. Seventy years after the fact, it is doubtful that additional evidence could be collected in what were, and largely remain, unpopulated areas.

Finally, we compare the 1949 tsunami with that generated by the recent Bodrum-Kos earthquake of 20 July 2017, approximately 240 km to the Southeast. Despite a significantly smaller moment of only 1.2×10^{26} dyn cm, the latter generated a locally stronger tsunami, with run-up reaching 1.9 m near Bodrum, and inundation up to 60 m. We note however that these effects were constrained to a number of specific locations involving small bays, coves and estuaries

(Doğan et al. 2019). By contrast, amplitudes recorded on tidal gauges did not exceed 20 cm, as reported and successfully modeled by Heidarzadeh et al. (2017).

In this context, the larger 2017 tsunami amplitudes are the results of site response effects, and not directly attributable to a different genesis at the source.

6. Discussion and Conclusions

We conducted a complete, modern seismological reassessment of the 1949 Chios earthquake, the second largest event of the past 100 years in the Central Aegean Sea. The event relocates to the basin separating Chios and Lesvos, in the general area of other modern relocations, but about 20 km NNE of the older ones, such as Galanopoulos' (1954); in this context, it is difficult to associate the 1949 event with the proposed Chios–Karaburun Fault. On the basis of individually read first motions, we confirm a normal faulting mechanism, expressing the "telephone book" extension during the transition from the strike-slip motion along the North Anatolian Fault to the East to the collision in the Southern Aegean to the Southwest. Mantle surface waves obtained at a number of teleseismic stations suggest a low-frequency moment of 7×10^{26} dyn cm, making this the second largest instrumentally recorded event in the Aegean. A complete recompilation of all available macroseismic data yields a distribution favoring rupture along the NNW-dipping plane. That structure complements the SSW-dipping fault which ruptured during the 2017 Lesvos earthquake to the North, on the other side of the Lesvos Basin (Kiratzi 2018). While this interpretation is in agreement with the description of the Northern Chios fault by Sboras (2011), as and listed by Karakaisis et al. (2010), the latter was described by Karakostas et al. (2010) as dipping to the South based on recent low-level seismicity.[1]

A field survey was carried out in order to collect memories of the event, and in particular of its tsunami, from surviving elderly witnesses. While most of them remembered the destruction caused by the earthquake, we could gather only a limited amount of quantitative data regarding the tsunami, which cannot help discriminate between the two possible fault planes of the 1949 earthquake. However, an important result is that both models provide an acceptable fit to the reported amplitudes. In this respect, the latter are compatible with the order of magnitudes of the maximum amplitudes η_{max} simulated from the dislocative sources derived from our seismological study, and we do not have to invoke ancillary sources such as underwater landslides. This is in contrast to the case of other historical tsunamis in the Aegean Sea, such as the 1956 Amorgos and 1948 Rhodos events, for which instances of spatially isolated excessive run-up amplitudes required generation by landslides (Okal et al. 2009; Ebeling et al. 2012).

Acknowledgements

We are grateful to Brian Ferris (Lower Hutt), Marjan Herak (Zagreb), and Eliška Zábranová (Prague) for access to historical records. Some figures were drafted using the GMT software (Wessel and Smith 1991). We thank two anonymous reviewers for their comments on the original draft of the paper. We salute the memory of Neşe Kânoğlu who shared with us the surveying in Turkey before her untimely passing in 2017.

Appendix

See Table 4.

[1] We note here an inconsistency in the numbering by Karakostas et al. (2010) of several of the clusters, between their Figs. 6 and 7 and their Table 1. This makes any reference to their work difficult and potentially unreliable.

Table 4

Macroseismic dataset compiled in this study

Number	Location		Latitude (°)	Longitude (°)	Epicentral distance (km)	Modified Mercalli intensity
	Town	Country				
1	Kardamyla	GR	38.538	26.085	28	IX
2	Karies	GR	38.391	26.093	41	IX
3	Oinousses	GR	38.524	26.222	22	IX
4	Egrigoros	GR	38.575	25.917	38	VIII$\frac{1}{2}$
5	Inousses	GR	38.515	26.221	23	VIII$\frac{1}{2}$
6	Küçükbahçe Bucağı	TR	38.561	26.390	18	VIII$\frac{1}{2}$
7	Amades	GR	38.571	26.037	29	VIII
8	Anbarseki Köyü	TR	38.614	26.523	21	VIII
9	Bozköy	TR	38.657	26.468	14	VIII
10	Chios	GR	38.358	26.121	43	VIII
11	İnecik	TR	38.551	26.567	28	VIII
12	Karaburun	TR	38.638	26.513	19	VIII
13	Keramos	GR	38.556	25.936	38	VIII
14	Kösedere	TR	38.554	26.554	27	VIII
15	Kourounia	GR	38.566	25.912	39	VIII
16	Marmaro	GR	38.544	26.108	26	VIII
17	Pispilounta	GR	38.527	25.951	38	VIII
18	Saip	TR	38.622	26.519	20	VIII
19	Spartounta	GR	38.545	25.992	34	VIII
20	Tepeboz	TR	38.661	26.447	12	VIII
21	Anavatos	GR	38.403	26.020	43	VII$\frac{1}{2}$
22	Armolia	GR	38.253	26.036	56	VII$\frac{1}{2}$
23	Birgi	TR	38.303	26.555	50	VII$\frac{1}{2}$
24	Çeşme	TR	38.324	26.303	43	VII$\frac{1}{2}$
25	Chalkio	GR	38.334	26.098	46	VII$\frac{1}{2}$
26	Coste	TR	38.356	26.311	39	VII$\frac{1}{2}$
27	Dapnonas	GR	38.347	26.080	45	VII$\frac{1}{2}$
28	Diefcha	GR	38.473	25.978	40	VII$\frac{1}{2}$
29	Eğlenhoca	TR	38.543	26.568	28	VII$\frac{1}{2}$
30	Exo Didima	GR	38.270	26.074	53	VII$\frac{1}{2}$
31	Flatsia	GR	38.239	26.079	56	VII$\frac{1}{2}$
32	Germiyan	TR	38.314	26.466	46	VII$\frac{1}{2}$
33	Hasseki	TR	38.664	26.417	10	VII$\frac{1}{2}$
34	Kalamoti	GR	38.234	26.046	58	VII$\frac{1}{2}$
35	Kallimasia	GR	38.293	26.101	50	VII$\frac{1}{2}$
36	Kampia	GR	38.572	25.982	33	VII$\frac{1}{2}$
37	Katarraktis	GR	38.265	26.103	53	VII$\frac{1}{2}$
38	Lagkada	GR	38.478	26.123	31	VII$\frac{1}{2}$
39	Ildır	TR	38.383	26.477	39	VII$\frac{1}{2}$
40	Neochori	GR	38.308	26.113	48	VII$\frac{1}{2}$
41	Parlak	TR	38.612	26.398	13	VII$\frac{1}{2}$
42	Pitious	GR	38.488	26.055	34	VII$\frac{1}{2}$
43	Salman	TR	38.592	26.384	14	VII$\frac{1}{2}$
44	Sarpıncık	TR	38.654	26.403	10	VII$\frac{1}{2}$
45	Sikiada	GR	38.464	26.124	32	VII$\frac{1}{2}$
46	Thimiana	GR	38.314	26.132	47	VII$\frac{1}{2}$
47	Tholopotami	GR	38.295	26.073	51	VII$\frac{1}{2}$
48	Varvasi	GR	38.357	26.135	42	VII$\frac{1}{2}$
49	Vrontados	GR	38.414	26.132	37	VII$\frac{1}{2}$
50	Yaylaköy	TR	38.574	26.455	19	VII$\frac{1}{2}$
51	Zifias	GR	38.327	26.080	47	VII$\frac{1}{2}$
52	Agios Georgios	GR	38.319	26.057	49	VII
53	Barbaros	TR	38.323	26.581	49	VII

Table 4 *continued*

Number	Location		Latitude (°)	Longitude (°)	Epicentral distance (km)	Modified Mercalli intensity
	Town	Country				
54	Çiftlik	TR	38.292	26.288	47	VII
55	Lithi	GR	38.331	26.001	50	VII
56	Foça	TR	38.670	26.758	38	VII
57	Reisdere	TR	38.304	26.437	46	VII
58	Uzunkuyu Bucağı	TR	38.285	26.551	51	VII
59	Viki	GR	38.580	26.012	30	VII
60	Volissos	GR	38.483	25.928	42	VII
61	Zeytinler	TR	38.284	26.561	52	VII
62	Alaçatı	TR	38.283	26.374	48	VI$\frac{1}{2}$
63	Balıklıova	TR	38.423	26.584	39	VI$\frac{1}{2}$
64	Elata	GR	38.287	25.989	55	VI$\frac{1}{2}$
65	Pirgi	GR	38.227	25.997	61	VI$\frac{1}{2}$
66	Vessa	GR	38.297	26.010	53	VI$\frac{1}{2}$
67	Mesta	GR	38.260	25.922	61	VI
68	Olimpi	GR	38.248	25.942	61	VI
69	Urla	TR	38.325	26.767	58	VI
70	Myrina	GR	39.881	25.083	168	V$\frac{1}{2}$
71	Patmos	GR	37.330	26.544	155	V
72	Samos	GR	37.772	26.974	119	V
73	Vathy	GR	37.746	27.004	123	V
74	Andros	GR	37.826	24.935	156	IV$\frac{1}{2}$
75	Karystos	GR	37.998	24.362	188	IV$\frac{1}{2}$
76	Ermoupoli	GR	37.440	24.933	186	IV
77	Ierissos	GR	40.415	23.833	285	IV
78	Kalymnos	GR	36.970	26.982	202	IV
79	Naxos	GR	37.103	25.391	196	IV
80	Ioulis	GR	37.657	24.336	209	III
81	Milos	GR	36.682	24.433	280	III
82	Mykonos	GR	37.455	25.350	163	III
83	Paros	GR	37.075	25.164	208	III
84	Seriphos	GR	37.163	24.477	236	III
85	Tinos	GR	37.538	25.172	165	III
86	Kymi	GR	38.652	24.102	193	II$\frac{1}{2}$
87	Skyros	GR	38.882	24.506	159	II$\frac{1}{2}$
88	Chalkida	GR	38.462	23.630	236	I
89	Istiaia	GR	38.965	23.148	277	I
90	Kassandreia	GR	40.062	23.384	294	I
91	Leros	GR	37.153	26.833	179	I
92	Samothraki	GR	40.456	25.577	204	I
93	Skiathos	GR	39.172	23.470	252	I
94	Skopelos	GR	39.097	23.714	230	I
95	Sykia	GR	40.034	23.938	252	I
96	Thasos	GR	40.768	24.691	268	I

References

Altınok, Y., Alpar, B., Özer, N., & Gazioğlu, C. (2005). 1881 and 1949 earthquakes in the Chios-Çeşme Strait (Aegean Sea) and their relation to tsunamis. *Natural Hazards and Earth System Sciences*, *5*, 717–725.

Ambraseys, N. N. (1998). Engineering seismology. *Earthquake Engineering and Structural Dynamics*, *17*, 1–105.

Ambraseys, N. N. (2001). Reassessment of earthquakes, 1900–1999, in the Eastern Mediterranean and the Middle East. *Geophysical Journal International*, *145*, 471–485.

Boatwright, J., & Choy, G. L. (1986). Teleseismic estimates of the energy radiated by shallow earthquakes. *Journal of Geophysical Research*, *91*, 2095–2112.

Caputo, R., Chatzipetros, A., Pavlides, S., & Sboras, S. (2012). The Greek database of seismogenic sources (GreDaSS): State-of-the-art for northern Greece. *Annals of Geophysics*, *55*, 859–894.

Charlier, C., & van Gils, J.-M. (1953). *Catalogue des stations séismologiques mondiales*. Uccle: Observatoire Royal de Belgique.

Chatzipetros, A., Kiratzi, A., Sboras, S., Zouros, N., & Pavlides, S. (2013). Active faulting in the north-eastern Aegean Sea islands. *Tectonophysics*, *507*, 106–122.

Doğan, G. G., Annunziato, A., Papadopoulos, G. A., Güler, H. G., Yalçıner, A. C., Çakır, T. E., et al. (2019). The 20th July 2017 Bodrum-Kos tsunami field survey. *Pure and Applied Geophysics*, *176*, 2925–2949.

Ebeling, C. W., Okal, E. A., Kalligeris, N., & Synolakis, C. E. (2012). Modern seismological reassessment and tsunami simulation of historical Hellenic Arc earthquakes. *Tectonophysics*, *530*, 225–239.

Ekström, G., & England, P. (1989). Seismic strain rates in regions of distributed continental deformation. *Journal of Geophysical Research*, *94*, 10231–10257.

Engdahl, E. R., & Villaseñor, A. (2002). Global seismicity: 1900–1999. *International earthquake and engineering seismology Part A* (pp. 665–690). New York: Elsevier.

Erkman, H. K. (1949). *23-7-1949 Karaburun (İzmir) zelzelesı* (19 pp.). Istanbul: Kandilli Observatory.

Field, E. H., Seligson, H. A., Gupta, N., Gupta, V., Jordan, T. H., & Campbell, K. (2005). Loss estimates for a Puente Hills Blind-Thrust earthquake in Los Angeles. *Earthquake Spectra*, *21*, 329–338.

Galanopoulos, A. (1954). Die Seismizität der Insel Chios. *Gerlands Beiträge zur Geophysik*, *63*, 253–264.

Geller, R. J. (1976). Scaling relations for earthquake source parameters and magnitudes. *Bulletin of the Seismological Society of America*, *66*, 1501–1523.

Godunov, S. K. (1959). Finite difference methods for numerical computations of discontinuous solutions of the equations of fluid dynamics. *Matematicheskii Sbornik*, *47*, 271–295.

Gutenberg, B., & Richter, C. F. (1942). Earthquake magnitude, intensity, energy and acceleration. *Bulletin of the Seismological Society of America*, *32*, 163–191.

Gutenberg, B., & Richter, C. F. (1954). *Seismicity of the earth and associated phenomena* (310 pp.). Princeton: Princeton University Press.

Heidarzadeh, M., Necmioğlu, O., Ishibe, T., & Yalçıner, A. C. (2017). Bodrum–Kos (Turkey–Greece) $M_w = 6.6$ earthquake and tsunami of 20 July 2017: A test for the Mediterranean tsunami warning system. *Geoscience Letters*, *4*(31), 11.

Kagan, Y. Y. (1991). 3-D rotation of double-couple earthquake sources. *Geophysical Journal International*, *106*, 709–716.

Kanamori, H. (1972). Mechanism of tsunami earthquakes. *Physics of the Earth and Planetary Interiors*, *6*, 346–359.

Karakaisis, G. F., Papazachos, C. B., & Scodilis, E. M. (2010). Seismic sources and main seismic faults in the Aegean and surrounding area. *Bulletin of the Geological Society of Greece*, *43*, 2026–2042.

Karakostas, V. G., Papadimitriou, E. E., Tranos, M. D., & Papazachos, C. B. (2010). Active seismotectonic structures in the area of Chios Island, North Aegean Sea, revealed from microseismicity and fault plane solutions. *Bulletin of the Geological Society of Greece*, *43*, 2064–2074.

Kiratzi, A. A. (2018). The 12 June 2017 $M_w = 6.3$ Lesvos Island (Aegean Sea) earthquake: Slip model and directivity estimated with finite-fault inversion. *Tectonophysics*, *724*, 1–10.

Labrouste, H., & Pinar, N. (1953). Etude microséismique des tremblements de terre du 23 juillet 1949 et du 13 août 1951 en Turquie. *Bull Inform UGGI*, *2*, 267–269.

Linkimer, L. (2008). Application of the kriging method to draw isoseismal maps of the significant 2002–2003 Costa Rica earthquakes. *Revista Geologica de America Central*, *38*, 119–134.

Mansinha, L. A., & Smylie, D. E. (1971). The displacement fields of inclined faults. *Bulletin of the Seismological Society of America*, *61*, 1433–1440.

McKenzie, D. P. (1972). Active tectonics of the Mediterranean region. *Geophysical Journal of the Royal Astronomical Society*, *30*, 109–185.

Melis, N. S., Barberopoulou, A., Frentzos, E., & Krassanakis, V. (2016). Scenario based tsunami wave height estimation towards hazard evaluation for the Hellenic coastline and examples of extreme inundation zones in South Aegean. *Geophysical Research Abstracts*, *18*, 1. (EGU2-16-11285-1, Vienna [abstract]).

Musson, R. M., Grünthal, G., & Stucchi, M. (2010). The comparison of macroseismic intensity scales. *Journal of Seismology*, *14*, 413–428.

Newman, A. V., & Okal, E. A. (1998). Teleseismic estimates of radiated seismic energy: The E/M_0 discriminant for tsunami earthquakes. *Journal of Geophysical Research*, *103*, 26885–26898.

Okal, E. A., & Borrero, J. C. (2011). The "tsunami earthquake" of 22 June 1932 in Manzanillo, Mexico: Seismological study and tsunami simulations. *Geophysical Journal International*, *187*, 1443–1459.

Okal, E. A., Fritz, H. M., Hamzeh, M. A., & Ghasemzadeh, J. (2015). Field survey of the 1945 Makran and 2004 Indian Ocean tsunamis in Baluchistan, Iran. *Pure and Applied Geophysics*, *172*, 3343–3356.

Okal, E. A., & Kirby, S. H. (2002). Energy-to-moment ratios for damaging intraslab earthquakes: Preliminary results on a few case studies. *USGS Open File Reports*, *02–328*, 127–131.

Okal, E. A., & Saloor, N. (2017). Historical tsunami earthquakes in the Southwest Pacific: An extension to $\Delta > 80^\circ$ of the energy-to-moment parameter Θ. *Geophysical Journal International*, *210*, 852–873.

Okal, E. A., Synolakis, C. E., Fryer, G. J., Heinrich, P., Borrero, J. C., Ruscher, C., et al. (2002). A field survey of the 1946 Aleutian tsunami in the far field. *Seismological Research Letters*, *73*, 490–503.

Okal, E. A., Synolakis, C. E., Uslu, B., Kalligeris, N., & Voukouvalas, E. (2009). The 1956 earthquake and tsunami in Amorgos, Greece. *Geophysical Journal International*, *178*, 1533–1554.

Okal, E. A., & Talandier, J. (1989). M_m: A variable period mantle magnitude. *Journal of Geophysical Research*, *94*, 4169–4193.

Papadopoulos, G. A. (2015). *Tsunamis in the European-Mediterranean region: From historical record to risk mitigation* (271 pp.). Amsterdam: Elsevier.

Papazachos, B., & Papazachou, C. (1997). *The earthquakes of Greece* (304 pp.). Thessaloniki: Ziti.

Pinar, N. (1950). Etude géologique et séismologique du tremblement de terre de Karaburun (Izmir) du 23 juillet 1949. *Revue de la Faculté des Sciences de l'Université d'Istamboul*, *15*, 363–375.

Sboras, S. (2011). *The Greek Database of Seismogenic Sources: Seismotectonic implications for North Greece*. PhD Thesis, University of Ferrara, 274 pp.

Schenková, Z., Schenk, V., Kalogeras, I., Pichl, R., Kottnauer, P., Papatsimba, C., et al. (2007). Isoseismal maps drawing by the kriging method. *Search Results*, *11*, 345–353.

Solov'ev, S. L., Solov'eva, O. N., Go, Ch. N., Kim, Kh. S., & Shchetnikov, N. A. (2013). *Tsunamis in the Mediterranean Sea, 2000 B.C.–2000 A.D*. (308 pp.). Dordrecht: Elsevier.

Storchak, D. A., Di Giacomo, D., Bondár, I., Engdahl, E. R., Harris, J., Lee, W. H. K., et al. (2013). Public release of the ISC-GEM global instrumental earthquake catalogue (1900–2009). *Seismological Research Letters*, *84*, 810–815.

Synolakis, C. E. (2003). Tsunami and seiche. In W.-F. Chen & C. Scawthron (Eds.), *Earthquake Engineering Handbook* (pp. 9_1–9_90). Boca Raton: CRC Press.

Synolakis, C. E., Bernard, E. N., Titov, V. V., Kânoğlu, U., & González, F. (2008). Validation and verification of tsunami numerical models. *Pure and Applied Geophysics*, *165*, 2197–2228.

Taymaz, T., Jackson, J., & McKenzie, D. (1991). Active tectonics of the north and central Aegean Sea. *Geophysical Journal International*, *106*, 433–490.

Titov, V. V., Kânoğlu, U., & Synolakis, C. E. (2016). Development of MOST for real-time tsunami forecasting. *Journal of Waterway, Port, Coastal, and Ocean Engineering*, *142*(6), 03116004.

Titov, V. V., Moore, C. W., Greenslade, D. J. M., Pattiaratchi, C., Badal, R., Synolakis, C. E., et al. (2011). A new tool for inundation modeling: Community Modeling Interface for Tsunamis (ComMIT). *Pure and Applied Geophysics*, *168*, 2121–2131.

Titov, V. V., & Synolakis, C. E. (1998). Numerical modeling of tidal wave runup. *Journal of Waterway, Port, Coastal, and Ocean Engineering*, *124*, 157–171.

Wessel, P., & Smith, W. H. F. (1991). Free software helps map and display data. *Eos Transactions American Geophysical Union*, *72*, 441, 445–446.

Wickens, A. J., & Hodgson, J. H. (1967). Computer re-evaluation of earthquake mechanism solutions, 1922–1962. *Publications of the Dominion Observatory, Ottawa*, *33*(1), 71.

Wysession, M. E., Okal, E. A., & Miller, K. L. (1991). Intraplate seismicity of the Pacific Basin, 1913–1988. *Pure and Applied Geophysics*, *135*, 261–359.

(Received May 28, 2019, revised December 18, 2019, accepted December 27, 2019, Published online January 30, 2020)